Gap states induce soft Fermi level pinning upon charge transfer at ZnO/molecular acceptor interfaces

Raphael Schlesinger,[1] Fabio Bussolotti,[2,3] Jinpeng Yang,[2,4] Sergey Sadofev,[1] Antje Vollmer,[5] Sylke Blumstengel,[1] Satoshi Kera,[2,3] Nobuo Ueno,[2] and Norbert Koch[1,5,*]

[1]*Humboldt-Universität zu Berlin, Institut für Physik & IRIS Adlershof, 12489 Berlin, Germany*

[2]*Department of Nanomaterial Science, Graduate School of Advanced Integration Science, Chiba University, Chiba 263–8522, Japan*

[3]*Institute for Molecular Sciene, Myodaiji, Okazaki 444–8585, Japan*

[4]*College of Physical Science and Technology, Yangzhou University, Jiangsu, 225009, China*

[5]*Helmholtz-Zentrum Berlin für Materialien und Energie GmbH, BESSY II, 12489 Berlin, Germany*

(Received 10 April 2019; revised manuscript received 21 May 2019; published 3 July 2019)

The deposition of strong molecular electron acceptors onto ZnO induces a substantial work function (ϕ) increase due to electron transfer from the inorganic semiconductor to the molecules. The ϕ increase results from two mechanisms: (i) a change of the surface band bending within ZnO and (ii) an interface dipole between the inorganic surface and the negatively charged acceptors. The molecule adsorption induced upward band bending in ZnO is, however, found to be limited to a few 100 meV, while the ϕ increase is significantly larger (up to 2.8 eV). We elucidate the origin of limited upward band bending by revealing a notable gap state density-of-states (GDOS) using high-sensitivity photoemission spectroscopy. Upon acceptor-induced upward band bending, the GDOS with a wide energy distribution becomes increasingly unoccupied. This, in turn, makes the interface dipole dominant and limits the ZnO surface band bending changes due to a "soft" pinning at the Fermi level.

DOI: 10.1103/PhysRevMaterials.3.074601

I. INTRODUCTION

Hybrid inorganic-organic semiconductor structures can benefit from the favorable properties of the two different material classes, enabling superior or different functionality. For example, inorganic semiconductors often exhibit high charge carrier mobility, sharp optical excitations, and superior structural definition, while organic semiconductors feature strong light-matter coupling, high luminescence yield, and facile chemical tunability. Regarding the electron energy levels in the bulk and at the surface, charge rearrangements within inorganic semiconductor are usually accompanied by surface band bending (or changes thereof), whereas organic semiconductors often exhibit flat energy levels throughout a thin film due to low charge carrier density and the closed-shell nature of the molecular orbitals, and thus no apparent surface states [1–4]. Among the numerous inorganic semiconductors, zinc oxide (ZnO) is of particular interest for (opto-)electronic devices due to its wide band gap of over 3 eV and thus transparency in the visible spectrum. Furthermore, its constituting elements are abundant. However, for many actual device structures, adjusting the energy level alignment at the inorganic/organic interface is necessary to achieve the desired functionality [5–8]. Upon proper design of the level alignment, though, combining ZnO with organic semiconductors has been shown to result in superior interfacial energy transfer and subsequent luminescence quantum yield [8].

Several studies have addressed the issue of energy level alignment tuning at interfaces with ZnO [7–12]. One approach consists of depositing a monolayer of a strong molecular acceptor (donor), and the concomitant interfacial charge transfer between ZnO and the molecules increases (decreases) the surface work function (ϕ). An organic semiconductor deposited on top then re-aligns its energy levels with respect to the modified ϕ, and level tuning between the inorganic and the organic semiconductor is achieved. It was proposed that the change in ϕ ($\Delta\phi$) is due to a superposition of two mechanisms: (i) a change in the surface band bending of the inorganic semiconductor ($\Delta\phi^{BB}$) and (ii) an interface dipole due to the charged molecules atop the inorganic surface ($\Delta\phi^{ID}$). In principle, $\Delta\phi^{BB}$ could reach the limits set by intrinsic Fermi level pinning at the valence and conduction band edges, respectively. This would correspond to the Fermi level (E_F) reaching the valence band maximum (VBM) or the conduction band minimum of the inorganic semiconductor. However, upward band bending upon molecular acceptor adsorption was found to be limited to only a few 100 meV [7], resulting in the formation of a much larger $\Delta\phi^{ID}$ to give the total $\Delta\phi$. In subsequent work, a finite surface state density (or gap state density-of-states, GDOS) of the inorganic semiconductor was suggested to be the cause of the undersized $\Delta\phi^{BB}$ [6,13–16]. Yet, details of the molecular adsorption induced band bending within semiconductors, notably ZnO, remain unclear, because the energy distribution and density of the GDOS, which seemingly play a key role, is elusive.

Here, we present a comprehensive study corroborating the mechanism of the limitation of $\Delta\phi^{BB}$ in ZnO, which can reasonably be extended to any semiconductor. Based on established electrostatic considerations [13], we show that besides the intrinsic ionized shallow donors of bulk ZnO, a second, albeit larger, charge density must be present at

*Corresponding author: norbert.koch@physik.hu-berlin.de

the ZnO surface, corresponding with states in the forbidden energy gap. Our high-sensitivity, low background ultraviolet photoemission spectroscopy (UPS) investigations of the energy gap region of three main-index ZnO faces elucidate the nature of those states and their relationship with $\Delta\phi^{BB}$ in ZnO upon the deposition of two different molecular acceptors. For all investigated surfaces, a notable GDOS with wide energy spread is found, up (or at least very close) to E_F. Thus, the notion of electron band tails extending far into the ZnO band gap region is substantiated [17–29]. Our findings for the GDOS wholly explain the observed behavior of acceptor-induced band bending changes in ZnO, and facilitate rationalizing the energy level alignment at hybrid inorganic/organic semiconductor interfaces in general.

II. EXPERIMENTAL METHODS

X-ray photoelectron spectroscopy (XPS) measurements were performed at the storage ring BESSY II (Berlin) at beamline PM4, experimental station SurICat (see Ref. [7] for details). Photon energies used were 610–620 eV. The low background UPS measurements were conducted using a high-precision UPS apparatus with an electron energy analyzer (MBS A-1) and monochromatized He I_α ($h\nu = 21.218$ eV) and Xe I_α radiation ($h\nu = 8.437$ eV) light sources. The light sources consist of a partly modified MBS M-1 monochromator (with an Al filter for He I_α and a LiF crystal filter for Xe I_α), as well as a MBS L-1 discharge lamp (He I_α) and an Omicron HIS 13 discharge lamp (Xe I_α) [29–31]. The intensity of the He I_β satellite ($h\nu = 23.087$ eV) was $\sim 5 \times 10^5$ lower than that of He I_α, and the intensity of other unwanted radiation was even lower than that of He I_β. All spectra were measured at normal emission with an acceptance angle of $\pm 18^\circ$. For measurements of the secondary electron cutoff the sample was biased to -10V to clear the analyzer work function. The binding energy refers to the Fermi level for both XPS and UPS spectra. ZnO single crystals were purchased from Tokyo Denpa. ZnO thin film samples were grown by molecular beam epitaxy on sapphire wafers. Highly *n*-doped crystals were $\sim 10^{20}\,cm^{-3}$ Ga doped ZnO$(000\bar{1})$, grown as described in Ref. [32]. The ZnO surfaces were cleaned by repeated cycles of Ar-ion sputtering and annealing (2 μA 500 V; 400 °C, see Ref. [7]), the last annealing step under 10^{-6} mbar O_2 for 10 min. Organic substances [2,3,5,6–tetrafluoro–7,7,8,8–tetracyano–quinodimethane (F4TCNQ), 1,4,5,8,9,12-hexaazatriphenylene-hexacarbonitrile (HATCN), and n-tetratetracontane (TTC)] were evaporated from resistively heated quartz crucibles. The amount of evaporated material (given as nominal thicknesses Θ) was monitored using a quartz crystal microbalance and set to the rate equivalent of about 1 Å/min using a density of 1.64, 1.60, and 0.82 g/cm^3 for F4TCNQ, HATCN, and TTC, respectively.

III. RESULTS

Two prototypical strong molecular electron acceptors, F4TCNQ and HATCN, were deposited onto different clean ZnO surfaces [ZnO(0001), ZnO$(10\bar{1}0)$ and ZnO$(000\bar{1})$]. The electron transfer into the surface-adsorbed acceptor layer strongly increased ϕ, accompanied by an upward surface band bending change in ZnO ($\Delta\phi^{BB}$), as noted in the introduction. Figures 1(a) and 1(b) display the evolution of both ϕ and the change of $\Delta\phi^{BB}$, the latter readily obtained from the shift of the ZnO core levels. Shown is the averaged shift of the O1*s* and Zn3*p* levels ΔE; selected spectra from which data in Fig. 1 were extracted are shown in Fig. S1 of the Supplemental Material [33]). We note that the slight differences of initial ϕ of up to ∼0.25 eV observed for the bare ZnO surfaces between different measurement series have two causes. First of all, the work function of a surface depends on its composition and details of its structure. For ZnO even slight (unintended) variations of the surface cleaning/conditioning process in UHV (see Sec. II) result in changes of structure and composition (e.g., surface hydroxyl loading) and thus variations in ϕ. Second, similar energy level shifts occur for ZnO upon irradiation with UV light over time [34]. Consequently, parameters such as ϕ reflect the properties of the sample under study, and are thus not intrinsic material constants but exhibit a range of values. For the same reason, also the magnitude of band bending observed in ZnO upon acceptor deposition exhibits a range of values for nominally identical but factually different samples. In return, for a number of such nominally identical samples we find varying ΔE, as indicated by the error bars (at maximum acceptor coverage) in Fig. 1(b). These variations, however, do not impact the generally valid following rationales.

As can be clearly seen, $\Delta\phi \gg \Delta E$, indicating that the major contribution to $\Delta\phi$ does not stem from $\Delta\phi^{BB}$, but rather from the interface dipole contribution $\Delta\phi^{ID}$. Note, $\Delta\phi^{BB}$ is not indicative of the final ZnO surface band bending, since the ZnO bands are already bent for the pristine surfaces. The final surface band bending relative to the crystal bulk is inferred from the ZnO core level position variation [*vide infra*, discussion of Fig. 1(c)]. The finding that $\Delta\phi^{BB}$ contributes little to $\Delta\phi$ cannot be rationalized in terms of an empty gap model, taking into account only the ZnO native shallow donors. Calculations for that case (natively doped ZnO and strong molecular acceptors), yield an expected $\Delta\phi^{BB}$ contribution to $\Delta\phi$ of 99% and concomitantly a $\Delta\phi^{ID}$ of only 1% [7], as represented in Fig. 2(a). This is in marked contrast to our experimental observation that $\Delta\phi^{BB}$ is typically less than 30% of $\Delta\phi$ (Fig. 1).

To resolve this discrepancy, a finite GDOS must be involved (at least) at the interface, so that pinning of the energy levels with respect to E_F (see, e.g., the Bardeen model [13]) upon upward band bending occurs. This can be understood from electrostatic considerations using Poisson's equation, as described in the following. The experimentally determined electrostatic potential variation across the ZnO/acceptor interface is depicted in Figs. 2(b) and 2(c), since the surface band bending is reliably measured by the ZnO core level shifts and core level positions [35]. The band bending inside ZnO is caused by ionized shallow donors N_D^+ (blue in Fig. 2). At the surface of ZnO the positive charge density ρ must be greatly enhanced (purple in Fig. 2) to continuously connect the regions inside and outside the ZnO crystal. The concentration of the native shallow donors of ZnO of $\sim 10^{17}\,cm^{-3}$ [36] is too low to be the only source of those ZnO surface charges [37], even if one considers a strongly enhanced doping concentration by one or two orders of magnitude. For instance, a

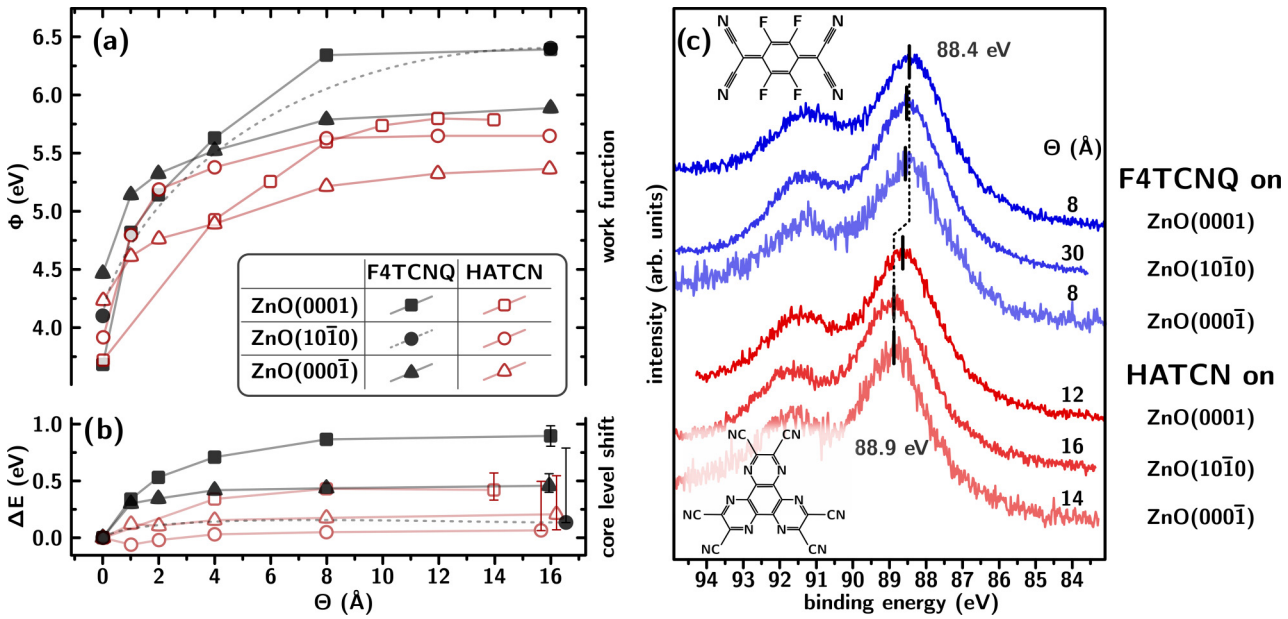

FIG. 1. Evolution of (a) the work function (ϕ) and (b) the acceptor adsorption-induced ZnO band bending changes upon F4TCNQ and HATCN adsorption on different faces of ZnO. The surface band bending change is determined from the core level shifts (ΔE) in the O1s and Zn3p spectra. The observed range of different core level shift sizes from different measurement series is indicated by error bars (for the respective highest molecular coverage Θ only). For all samples the work function shift ($\Delta\phi$) by far surpasses the core level shift, implying the existence of a significant complementary interface dipole ($\Delta\phi^{\mathrm{ID}}$). (c) Zn3p core level spectra of ZnO with adsorbed molecular electron acceptors (saturation of $\Delta\phi$ reached), indicative of the final adsorption-induced surface band bending change ($\Delta\phi^{\mathrm{BB}}$). Compared to the overall work function changes $\Delta\phi$ (a), the Zn3p core level positions are almost constant. This evidences the limits of $\Delta\phi^{\mathrm{BB}}$ in ZnO upon molecular acceptor adsorption.

∼threefold increased doping was observed at the surface due to hydrogen diffusion into ZnO [38]. As the native shallow donor density is insufficient for the small $\Delta\phi^{\mathrm{BB}}$ and the VBM was measured ∼2.5 eV below E_{F} after acceptor deposition, it is tangible that the source of the surface charges is within the forbidden energy gap region, i.e., the GDOS. That GDOS could be an intrinsic property of ZnO, e.g., discrete levels due to traps [39,40] or surface states [41–45], or a continuum of electron band tails induced by disorder [17–28]. Alternatively, the GDOS could be induced extrinsically by the molecular adsorbate layer, e.g., an induced density of interface states (IDIS), or due to hybridization of the molecular states with the ZnO bands [46–49]. The IDIS model considers the induced (by interface formation) density of states and that the charge neutrality levels on either side of the interface align. Our rationales are similar to this in that they consider density of states in the gap irrespective of its physical origin, and then apply Fermi-Dirac statistics to infer occupation and charge densities. All of these possibilities for GDOS are very different in nature, with respect to their influence on charge transport, the position in the crystal (surface *versus* bulk), as well as the localization of the wave functions [50–52]. While the mere presence of GDOS suffices to qualitatively explain the interfacial energy levels, other device-relevant parameters critically require knowing the origin and distribution of the GDOS.

To obtain detailed information on the GDOS, we performed ultralow-background UPS experiments. Figure 3 shows the corresponding spectra for the topmost valence and gap region of clean ZnO(0001), ZnO(10$\bar{1}$0), and ZnO(000$\bar{1}$) surfaces, as well as of a highly n-doped (by Ga atoms) ZnO(000$\bar{1}$) for comparison. The data are shown on a linear (left) and a logarithmic intensity scale (right) to present the full dynamic range of the measurements. The photoemission low-energy onsets of the ZnO valence band (valence band maxima) are indicated by red marks, representing the onset of the forbidden energy gap region. Upon inspecting the logarithmic plot in Fig. 3 it becomes evident that a finite GDOS is indeed present for all investigated ZnO surfaces. On ZnO(0001) one observes even a structured feature crossing E_{F}, which is not part of the GDOS, but rather the partially filled conduction band, due to the pronounced downward surface band bending at this surface [53,54]. A similar feature at E_{F} is also seen for the Ga-doped ZnO(000$\bar{1}$). In contrast to the ZnO(0001) surface, we do not attribute this feature to a partially filled conduction band, since the VBM is at ∼2.8 eV binding energy, i.e., the ZnO energy gap would appear too narrow by ∼0.5 eV. Rather, we suspect that this feature is induced by the UV irradiation used in UPS [34] (see Fig. S2 and discussion in the Supplemental Material [55]). Apart from the two distinct features observed at E_{F}, the actual GDOS is continuous in energy virtually throughout the gap and largely featureless, and we thus attribute it to originate from (disorder induced) electron band tails. For the ZnO(10$\bar{1}$0) surface, the GDOS seems to vanish even before reaching E_{F} [indicated by Δ in Fig. 3(b)]; however, we note that it actually intersects the instrumental signal background, and thus the GDOS may extend up to E_{F}, yet with a density lower than accessible in experiment. The notion of band tails is further corroborated by the fact that the tail of the Ga doped sample is steeper (larger

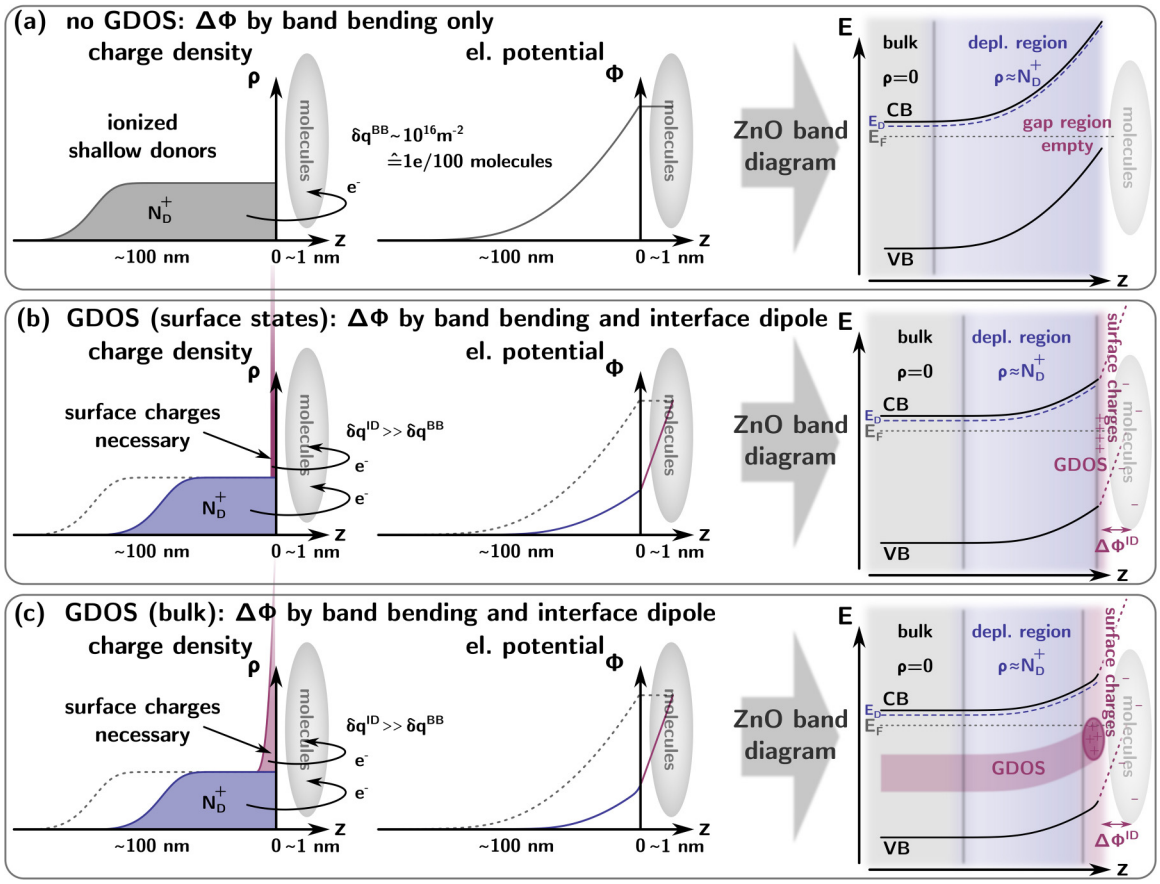

FIG. 2. Schematic illustration of charge density (ρ), electrostatic potentials (el. potential), and resulting energy level diagrams for acceptors adsorbed on ZnO. (a) The scenario where the work function change originates only from depletion of the native ZnO dopants ($N_D \approx 10^{17}$ cm^{-3}; binding energy E_D), i.e., the "empty gap model". This would result in $\Delta\phi$ almost exclusively being due to band bending (>99%). (b) and (c) The same scenario including the presence of GDOS, in which the interface dipole dominates. This requires an additional surface charge density (purple), provided for by the GDOS. (b) depicts the situation if GDOS originates from surface states and (c) from GDOS present also in the bulk.

slope in logarithmic scale) than the one of the natively doped sample, which is expected from the higher (doping induced) disorder in the Ga doped sample. Theoretical work on the DOS [$g(E)$] of electron band tails as function of energy E, as in Refs. [20,21], predict a multitude of allowed functional forms of the tails ranging from $g(E) \sim |E|^{1.5}\exp(-\text{const}\,|E|^{0.5})$ [56] to $g(E) \sim |E|^{3}\exp(-\text{const}\,|E|^{2})$ [57], depending on the correlation length of the disorder. For ZnO(10$\bar{1}$0) and the Ga doped ZnO(000$\bar{1}$) we find that the GDOS decreases exponentially (linear slope in logarithmic scale), whereas for the natively doped ZnO(000$\bar{1}$) and ZnO(0001) this is not obviously the case. Note that the precise shape of the GDOS is delicately preparation sensitive, since for the nominally same surface cleaning procedure also slight differences in the GDOS and initial surface band bending were observed [see, e.g., ZnO(0001) and ZnO(000$\bar{1}$) baselines in Figs. 3–5], phenomenologically similar to what we discussed for the ZnO ϕ above. Particularly, the "bump" between 2 and 3 eV binding energy in the ZnO(0001) spectrum could also be due to residual contaminations on the surface, since a similar shape was observed in the photoemission spectra of an only once sputtered, and thus not perfectly clean, ZnO(000$\bar{1}$) surface.

We further want to demark the present results from Urbach tails. Urbach tails reported for ZnO extend only a few 100 meV into the gap [58–65], but not 2 eV as observed here. Therefore, if any, only the energy region adjacent within a few 100 meV to the VBM (red onset markers in Fig. 3) could be related to what is commonly referred to as the Urbach tail.

Based on the evidence of an intrinsic, yet sample surface dependent, ZnO GDOS, one can already comprehensively understand the behavior of the smaller than expected acceptor adsorption induced $\Delta\phi^{BB}$, as follows. First, electron transfer from the shallow donors into the acceptors leads to band bending changes in ZnO, thus rigidly shifting all energy levels upwards. As soon as E_F intersects with the occupied GDOS, those states become unoccupied and stop further upward band bending. In the case of the ZnO(0001) surface, where the partially filled conduction band is below E_F due to initially pronounced downward surface band bending (see above), these states are emptied as well, also contributing to reduced adsorption induced $\Delta\phi^{BB}$. Depending on whether the GDOS exists only at the surface [Fig. 2(b)] or also in the bulk ZnO crystal [Fig. 2(c)], the density of charged GDOS will change abruptly or smear out towards the bulk crystal

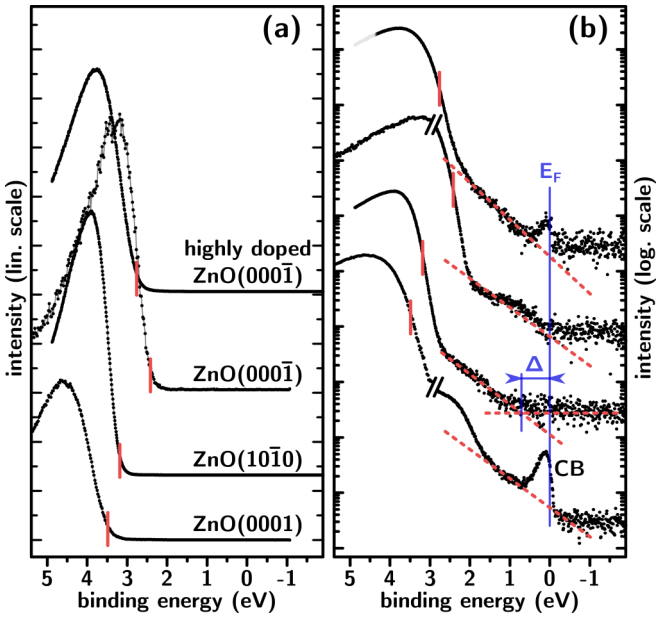

FIG. 3. Valence and energy gap region He I_α UPS spectra of differently terminated clean ZnO surfaces, plotted on (a) linear and (b) logarithmic intensity scale. The onset positions of the valence band (VBM) are indicated with red markers. The breaks in (b) indicate concatenation of individually measured spectra. On logarithmic intensity scale a continuous (decaying towards E_F) photoemission intensity in the forbidden energy gap region of ZnO (GDOS) is visible. The ZnO(0001) face exhibits a pronounced feature at the Fermi level due to downward band bending and partial occupation of the conduction band (CB). The feature at E_F of the highly doped ZnO(000$\bar{1}$) sample is due to He I_α UV light induced defects and discussed in the Supplemental Material. For ZnO(10$\bar{1}$0) and the highly Ga-doped ZnO(000$\bar{1}$) faces, the band tails fall off approximately exponentially (linear slope in logarithmic scale; indicated by dashed lines).

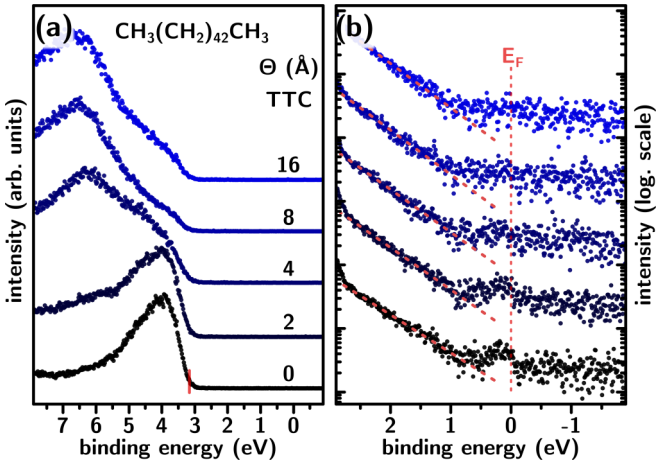

FIG. 4. Valence region spectra of TTC (measured with He I_α) with incrementally increased thickness on ZnO(000$\bar{1}$) plotted in (a) on a linear and (b) on a logarithmic intensity scale. The wide bandgap of TTC allows us to observe the ZnO bandgap region upon adsorption without being superimposed by TTC features. The bare ZnO spectrum features a photoemission onset of >3 eV with an exponential tail (linear slope in logarithmic plot) in the gap region. Upon deposition of TTC the intrinsic ZnO GDOS persists with respect to position and slope (in logarithmic scale).

according to Fermi Dirac statistics and a continuous potential curve. Importantly, no abrupt pinning occurs, since the final adsorption induced ZnO band positions vary by about 0.5 eV [see Zn3p core level positions in Fig. 1(c)]. However, this can be explained by the fact that the GDOS is rather low near E_F and gradually becomes larger when approaching the valence band, rendering the E_F pinning "soft" instead of abrupt. Therefore, the relative position of E_F within the GDOS slightly varies with the required amount of charge transfer to yield the $\Delta\phi^{ID}$ that electronically equilibrates the interface. Consistently, the adsorption induced final Zn3p core level positions, representing the absolute surface band bending, are found in the same order [see markers in Fig. 1(c)] as the corresponding final ϕ, thus indicative of the required amount of charge transfer. It is also noteworthy that the amount of transferred charge across the interface depends on the ϕ values of the clean ZnO surface. As can be seen from Fig. 1(a), initial ϕ values of ZnO(0001) are consistently lower than those of the other two surfaces, implying an overall larger amount of transferred charge. This is fully in line with the observation that the final ϕ *and* ΔE values of acceptor/ZnO(0001) surfaces are consistently higher than those for the other two surface terminations. Furthermore, the adsorption induced band bending should to some degree be suppressible by a higher doping concentration inside ZnO, as observed experimentally [15]. Yet, whether this is a sizeable effect depends on how much charge transfer is required and how large the charge reservoir from GDOS

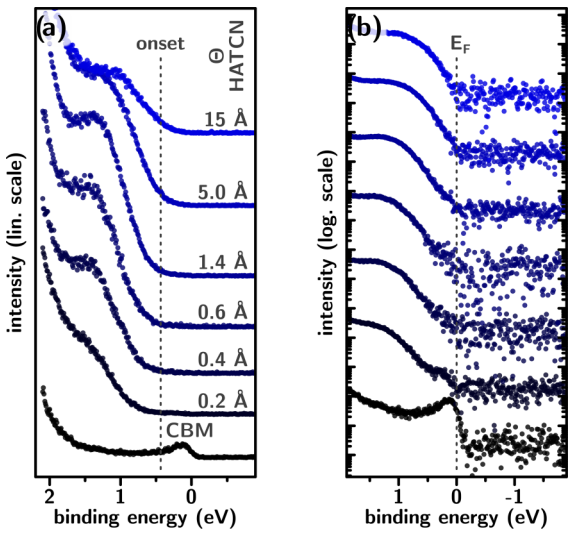

FIG. 5. Valence region spectra (measured with Xe I_α) of incrementally increased thickness of HATCN on ZnO(0001) plotted in (a) on a linear and (b) on a logarithmic intensity scale. Even for the smallest coverage the induced upward band bending is sufficiently strong to completely empty the ZnO conduction band (below E_F initially). For higher coverages a feature arises at ∼1.5 eV BE. Upon further increasing the coverage that feature becomes attenuated, indicative of it being only present at the interface.

actually is. We have to point out that a direct quantitative comparison of the acceptor-induced band bending change [ΔE from Fig. 1(b)] and the apparent GDOS shape and magnitude [Fig. 3(b)] cannot be made. These two sets of experiments were performed in different experimental setups (measuring core levels in the setup used for ultralow-background UPS was not possible), and thus details of sample surface properties (ϕ and actual GDOS) most likely vary (see discussions of surface cleaning procedures and sample properties above).

Note that the transition from depleting the ZnO donors to depleting the occupied GDOS has strong implications for the charge density at the hybrid interface and the required charge transfer [see Figs. 2(b) and 2(c)]. For the present experiments the charge transfer from GDOS should be 1–100 times that of the entire subsurface depletion region. This is reasonable, considering the wider spatial distance between charge and countercharge if the charge transfer originates from the native dopants. Thus, band bending is much more efficient in changing ϕ per transferred charge. Also, we want to point out that due to the "soft" pinning at the GDOS the width of the depletion region of ZnO will be rather universally around 100 nm upon acceptor deposition. This is due to the fact that in depletion approximation the width of the depletion region scales only as the square root of the surface band bending potential shift, which in turn, due to wide energy distribution of the GDOS, varies by only $\sim$0.5 eV.

While the aforementioned findings already explain the observed energy levels and their changes, acceptor adsorption may induce additional GDOS, which would add up to the effect of the intrinsic ZnO GDOS. Unfortunately, experimentally determining acceptor-induced GDOS is compromised by the fact that the energy region of interest is superimposed by the occupied molecular states, or states due to hybridization of the molecule and ZnO after charge transfer (see, e.g., Figs. 2 and 5 in Ref. [7] and HATCN/ZnO discussed below). To test this possibility within an experimentally accessible framework, we deposited the inert, wide-gap saturated hydrocarbon TTC (as a model on the ZnO(000$\bar{1}$) surface (see Fig. 4). By using TTC, for which interfacial charge transfer can be ruled out, the ZnO bandgap region is not obscured by molecular states in UPS spectra. We find that upon TTC adsorption the intrinsic ZnO GDOS becomes attenuated as expected, but its shape remains identical. This shows that the intrinsic ZnO GDOS indeed persists, at least upon adsorption of molecules that do not induce charge transfer. This further corroborates that the GDOS identified here acts as a limitation for $\Delta\phi^{\mathrm{BB}}$ at such hybrid interfaces and thus strongly influences the energy level alignment.

Despite the conceptual generality of the presented findings on the ZnO GDOS, the precise modalities of the energy level alignment at a ZnO-acceptor interface may still be governed by states formed on either side of the interface and/or extending across the interface. Indeed, upon performing low background UPS for incremental depositions of HATCN onto ZnO one finds additional intensity arising in the ZnO gap region, whose tail extends to E_{F} (see Fig. 5). Further increasing the coverage attenuates this feature, indicative of it being present only at the interface, thus most likely due to negatively charged HATCN molecules (partially filled lowest unoccupied molecular orbital level). Yet, it becomes clear through these data that eventual molecule-induced changes of semiconductor surface GDOS, and thus pinning behavior, are barely accessible experimentally, except for select cases (e.g., TTC above).

Despite the achievement of the present study to explain the interfacial energy levels and their changes for molecular acceptors on ZnO, further work is needed to develop a concise quantitative framework based on the present experimental findings. This includes unraveling whether the intrinsic GDOS is a surface or bulk property, what states it is derived from, and how localized/delocalized the corresponding wave functions are. Furthermore, knowledge of the photoemission cross sections is imperative to link the observed photoemission intensities to GDOS on a quantitative scale and to also include the peculiarities of the bonding and electronic states of a specific acceptor to the individual ZnO surface as discussed in Ref. [29]. Finally, from an application point of view, it is necessary to take into account that the GDOS will certainly depend on surface cleanliness, preparation procedures, and details of the surface structure. Nevertheless, the presence and persistence of the intrinsic ZnO GDOS represents a fundamental limitation for upward band bending induced by acceptor adsorption on ZnO.

IV. CONCLUSIONS

We demonstrated that the upward surface band bending in ZnO induced by molecular acceptor adsorption is limited to $\sim$0.5 eV. Concomitantly, a substantial interface dipole is formed to yield the overall work function change, which implies a notable positive charge density at the ZnO surface. Since the native shallow donor density of ZnO is insufficient to provide this surface charge, we conclude that a GDOS must be present. With high-sensitivity photoemission measurements of the ZnO energy gap region, a GDOS throughout the gap is indeed found for the three primary ZnO surface orientations. The origin of these gap states is attributed to disorder induced electron band tails. Upon electron transfer to the molecular acceptors, the GDOS acts as an electron reservoir that is sufficient to limit the magnitude of upward band bending within ZnO. Notably, due to the comparably low density of the GDOS and its wide energy distribution, upward band bending is not abruptly stopped, i.e., strongly pinned, but the E_{F}-pinning proceeds in a "soft" manner. With the illustrative examples provided here for ZnO, the charge re-distribution and energy level alignment, particularly the interplay of induced surface band bending changes and interface dipoles, at interfaces between inorganic semiconductors and molecular electron acceptors and donors can be rationalized, and eventually be exploited when the GDOS can be controlled.

ACKNOWLEDGMENTS

This work was supported by the Deutsche Forschungsgemeinschaft (DFG) - Projektnummer 182087777 - SFB 951, the JSPS-Global COE Program by Ministry of Education,

Culture, Sports, Science and Technology (MEXT) of Japan (Grant No. G03), Advanced School for Organic Electronics at Chiba University, and in part by JSPS KAKENHI (Grant No. JP24245034).

[1] H. Ishii, N. Hayashi, E. Ito, Y. Washizu, K. Sugi, Y. Kimura, M. Niwano, Y. Ouchi, and K. Seki, Phys. Status Solidi A **201**, 1075 (2004).
[2] T. Chass, C. I. Wu, I. G. Hill, and A. Kahn, J. Appl. Phys. **85**, 6589 (1999).
[3] I. G. Hill, A. J. Mäkinen, and Z. H. Kafafi, J. Appl. Phys. **88**, 889 (2000).
[4] J. Hwang, A. Wan, and A. Kahn, Mater. Sci. Eng. Rep. **64**, 1 (2009).
[5] M. T. Greiner, M. G. Helander, W.-M. Tang, Z.-B. Wang, J. Qiu, and Z.-H. Lu, Nat. Mater. **11**, 76 (2012).
[6] A. Klein, Thin Solid Films **520**, 3721 (2012).
[7] R. Schlesinger, F. Bianchi, S. Blumstengel, C. Christodoulou, R. Ovsyannikov, B. Kobin, K. Moudgil, S. Barlow, S. Hecht, S. R. Marder, F. Henneberger, and N. Koch, Nat. Commun. **6**, 6754 (2015).
[8] R. Schlesinger, Y. Xu, O. T. Hofmann, S. Winkler, J. Frisch, J. Niederhausen, A. Vollmer, S. Blumstengel, F. Henneberger, P. Rinke, M. Scheffler, and N. Koch, Phys. Rev. B **87**, 155311 (2013).
[9] M. Timpel, M. V. Nardi, S. Krause, G. Ligorio, C. Christodoulou, L. Pasquali, A. Giglia, J. Frisch, B. Wegner, P. Moras, and N. Koch, Chem. Mater. **26**, 5042 (2014).
[10] F. Piersimoni, R. Schlesinger, J. Benduhn, D. Spoltore, S. Reiter, I. Lange, N. Koch, K. Vandewal, and D. Neher, J. Phys. Chem. Lett. **6**, 500 (2015).
[11] P. Winget, L. K. Schirra, D. Cornil, H. Li, V. Coropceanu, P. F. Ndione, A. K. Sigdel, D. S. Ginley, J. J. Berry, J. Shim, H. Kim, B. Kippelen, J.-L. Brédas, and O. L. A. Monti, Adv. Mater. **26**, 4711 (2014).
[12] A. Calzolari, A. Ruini, and A. Catellani, J. Am. Chem. Soc. **133**, 5893 (2011).
[13] J. Bardeen, Phys Rev **71**, 717 (1947).
[14] T. Schultz, R. Schlesinger, J. Niederhausen, F. Henneberger, S. Sadofev, S. Blumstengel, A. Vollmer, F. Bussolotti, J.-P. Yang, S. Kera, K. Parvez, N. Ueno, K. Müllen, and N. Koch, Phys. Rev. B **93**, 125309 (2016).
[15] T. Schultz, J. Niederhausen, R. Schlesinger, S. Sadofev, and N. Koch, J. Appl. Phys. **123**, 245501 (2018).
[16] F. Zu, P. Amsalem, M. Ralaiarisoa, T. Schultz, R. Schlesinger, and N. Koch, ACS Appl. Mater. Interface **9**, 41546 (2017).
[17] P. A. Fedders, D. A. Drabold, and S. Nakhmanson, Phys. Rev. B **58**, 15624 (1998).
[18] F. Urbach, Phys. Rev. **92**, 1324 (1953).
[19] K. Boubaker, Eur. Phys. J. Plus **126**, 1 (2011).
[20] B. I. Halperin and M. Lax, Phys. Rev. **148**, 722 (1966).
[21] S. John, M. Y. Chou, M. H. Cohen, and C. M. Soukoulis, Phys. Rev. B **37**, 6963 (1988).
[22] S. John, C. Soukoulis, M. H. Cohen, and E. N. Economou, Phys. Rev. Lett. **57**, 1777 (1986).
[23] N. Mott, Adv. Phys. **16**, 49 (1967).
[24] B. Sadigh, P. Erhart, D. Åberg, A. Trave, E. Schwegler, and J. Bude, Phys. Rev. Lett. **106**, 027401 (2011).
[25] T. H. Nguyen and S. K. O'Leary, J. Appl. Phys. **88**, 3479 (2000).
[26] S. K. O'Leary, J. Mater. Sci. Mater. Electron. **15**, 401 (2004).
[27] H.-C. Wu, Y.-C. Peng, and C.-C. Chen, Opt. Mater. **35**, 509 (2013).
[28] A. D. Mirlin, Phys. Rep. **326**, 259 (2000).
[29] J.-P. Yang, F. Bussolotti, S. Kera, and N. Ueno, J. Phys. D **50**, 423002 (2017).
[30] T. Sueyoshi, H. Fukagawa, M. Ono, S. Kera, and N. Ueno, Appl. Phys. Lett. **95**, 183303 (2009).
[31] N. Ueno, T. Sueyoshi, F. Bussolotti, and S. Kera, in *Electronic Processes in Organic Electronics*, Springer Series in Materials Science, Vol. 209, edited by H. Ishii, K. Kudo, T. Nakayama, and N. Ueno (Springer, Japan, 2015).
[32] S. Sadofev, S. Kalusniak, P. Schäfer, and F. Henneberger, Appl. Phys. Lett. **102**, 181905 (2013).
[33] See Supplemental Material at http://link.aps.org/supplemental/10.1103/PhysRevMaterials.3.074601 for secondary electron cutoff, O1*s* and Zn3*p* core level regions of clean and ca. monolayer covered ZnO surfaces.
[34] K. Jacobi, G. Zwicker, and A. Gutmann, Surf Sci **141**, 109 (1984).
[35] There is some uncertainty of the core level positions due to slight UV irradiation induced energy level shifts within ZnO (see the Supplemental Material) and screening effects due to the extra charge density at the surface. However, this does not change the general fact that $\Delta\phi \gg \Delta\phi^{\mathrm{BB}}$.
[36] E. V. Lavrov, F. Herklotz, and J. Weber, Phys. Rev. B **79**, 165210 (2009).
[37] E. Arijs, F. Cardon, and W. Maenhout-van der Vorst, J. Solid State Chem. **6**, 319 (1973).
[38] F. Traeger, M. Kauer, C. Wöll, D. Rogalla, and H.-W. Becker, Phys. Rev. B **84**, 075462 (2011).
[39] J. Bang, H. Yang, and P. H. Holloway, Nanotechnology **17**, 973 (2006).
[40] J. Schmal, J. Non-Cryst. Solids **198**, 387 (1996).
[41] T. Okamura, Y. Seki, S. Nagakari, and H. Okushi, Jpn. J. Appl. Phys. **31**, 3218 (1992).
[42] R. Girard, O. Tjernberg, G. Chiaia, S. Söderholm, U. Karlsson, C. Wigren, H. Nylén, and I. Lindau, Surf. Sci. **373**, 409 (1997).
[43] R. Leysen, H. van Hove, J. Marien, and J. Loosveldt, Phys. Status Solidi A **11**, 539 (1972).
[44] A. Rizzi and H. Lüth, Il Nuovo Cimento D **20**, 1039 (1998).
[45] F. Garcia-Moliner and F. Flores, J. Phys. C **9**, 1609 (1976).
[46] H. Vázquez, F. Flores, R. Oszwaldowski, J. Ortega, R. Pérez, and A. Kahn, Appl. Surf. Sci. **234**, 107 (2004).
[47] H. Vázquez, R. Oszwaldowski, P. Pou, J. Ortega, R. Pérez, F. Flores, and A. Kahn, Europhys. Lett. **65**, 802 (2004).
[48] F. Flores and C. Tejedor, J. Phys. C **20**, 145 (1987).
[49] M. G. Betti, A. Kanjilal, C. Mariani, H. Vázquez, Y. J. Dappe, J. Ortega, and F. Flores, Phys. Rev. Lett. **100**, 027601 (2008).
[50] D. Redfield, Adv. Phys. **24**, 463 (1975).
[51] P. W. Anderson, D. J. Thouless, E. Abrahams, and D. S. Fisher, Phys. Rev. B **22**, 3519 (1980).

[52] C. M. Soukoulis and E. N. Economou, Waves Random Media **9**, 255 (1999).
[53] K. Ozawa and K. Mase, Phys. Rev. B **83**, 125406 (2011).
[54] M. G. Betti, V. Corradini, G. Bertoni, P. Casarini, C. Mariani, and A. Abramo, Phys. Rev. B **63**, 155315 (2001).
[55] See Supplemental Material at http://link.aps.org/supplemental/10.1103/PhysRevMaterials.3.074601 for effect of extended UV irradiation on the low BE valence electronic structure of ZnO($000\bar{1}$).
[56] J. L. Cardy, J. Phys. C **11**, L321 (1978).
[57] S. John and M. J. Stephen, J. Phys. C **17**, L559 (1984).
[58] Y. Natsume, H. Sakata, and T. Hirayama, Phys. Status Solidi A **148**, 485 (1995).
[59] N. R. Aghamalyan, I. A. Gambaryan, E. K. Goulanian, R. K. Hovsepyan, R. B. Kostanyan, S. I. Petrosyan, E. S.Vardanyan, and A. F. Zerrouk, Semicond. Sci. Technol. **18**, 525 (2003).
[60] Z. Xu, Q.-R. Zheng, and G. Su, Phys. Rev. B **85**, 075402 (2012).
[61] S. Dutta, S. Chattopadhyay, M. Sutradhar, A. Sarkar, M. Chakrabarti, D. Sanyal, and D. Jana, J. Phys.: Condens Matter **19**, 236218 (2007).
[62] H. Tang, F. Lévy, H. Berger, and P. E. Schmid, Phys. Rev. B **52**, 7771 (1995).
[63] M. Girtan and G. Folcher, Surf. Coat. Technol. **172**, 242 (2003).
[64] T. Shioda, S. Chichibu, T. Irie, H. Nakanishi, and T. Kariya, J. Appl. Phys. **80**, 1106 (1996).
[65] M. Schmidt, A. Schoepke, L. Korte, O. Milch, and W. Fuhs, J. Non-Cryst. Solids **338–340**, 211 (2004).